ELSEVIER

Thermochimica Acta 318 (1998) 177–186

thermochimica acta

Thermal and structural studies of amide complexes of transition metal(II) chlorides. II: Kinetics

Aubrey N. Nelwamondo[a], Desmond J. Eve[b], Michael E. Brown[b,*]

[a] *Department of Chemistry, University of Fort Hare, Alice, South Africa*
[b] *Department of Chemistry, Rhodes University, Grahamstown, 6140, South Africa*

Received 15 July 1997; accepted 2 September 1997

Abstract

The possibility of correlating the kinetic parameters for the thermal decompositions of a series of $NiLCl_2$ complexes, where L=*N*-methylformamide (*nmf*), *N*-methylacetamide (*nma*) or acetamide (*aa*), with the nature (steric and electronic effects) of the coordinated ligands and the strengths of the metal–ligand bonds has been explored. The rates of removal of L in single endothermic processes were measured using isothermal TG in nitrogen.

Plots of α against time are deceleratory and are best described by either the R2 or R3 expressions. An empirical (B2) expression: $v_r=1-(kt)^b$, was introduced to give the best description of the results for the Ni(*nma*)Cl_2 complex.

Comparable E_a values were obtained using various isothermal and non-isothermal methods of analysis. E_a values for the $NiLCl_2$ system (calculated using the R3 model) generally increased with an increase in basicity of the amide ligand:

N-methylformamide $\sim$ acetamide $<$ *N*-methylacetamide

E_a values were found to be lower than the corresponding decomposition enthalpies (ΔH_L), indicating that cleavage of the nickel–amide bond could be the rate-controlling event. The order of E_a values was found not to coincide with that of the ΔH_L values. Extrapolated onset temperatures (T_e) and temperatures at maximum decomposition rate (T_{max}) were determined from TG and DSC curves. No simple correlation was found between E_a, ΔH_L, T_e or T_{max} and the spectral properties of the complexes. © 1998 Elsevier Science B.V.

Keywords: Activation energies; Amide complexes; Isothermal TG; Kinetics; Nickel(II)

1. Introduction

Studies of the decomposition stoichiometry of a series of amide complexes of transition metal(II) chlorides [1] showed that in a nitrogen atmosphere the pseudooctahedral $NiLCl_2$ complexes, where L=*N*-methylformamide (*nmf*), *N*-methylacetamide (*nma*) or acetamide (*aa*), decomposed in a single endothermic step

$$NiLCl_2(s) \rightarrow NiCl_2(s) + L(g)$$

The possibility of correlating the kinetic parameters for such reactions with the nature (steric and electronic effects) of the coordinated ligands and the strengths of the metal–volatile ligand bonds has been explored. The kinetics of the thermal decompositions of the $NiLCl_2$ complexes were studied by following the mass

*Corresponding author. E-mail: chmb@warthog.ru.ac.za

PII S0040-6031(98)00342-6

losses for the removal of L using isothermal TG. The criteria used for selection were that there should be no melting (detected using DSC) and no apparent ligand decomposition (from programmed temperature TG).

2. Experimental

2.1. Materials

The preparation of the complexes selected for kinetic study has been reported elsewhere [1].

2.2. Equipment and procedures

Perkin–Elmer Series-7 TG and DSC equipment [1] was used. Heating to the selected isothermal reaction temperature for TG was at 200°C min^{-1}. Mass losses were converted to fractional reaction,

$$\alpha = (m_0 - m)/(m_0 - m_f)$$

where m_0 is the initial mass of sample, m the mass at time t and m_f the final mass. (v=dα/dt) values were calculated using a nine-point Savitsky–Golay function [2]. Where necessary, a correction for the short '*warming-up*' period (t_0) required by the instrument to reach the isothermal reaction temperature was made, so that

$$t = t_e - t_0 \quad \text{and} \quad \alpha = (\alpha_e - \alpha_0)/(1 - \alpha_0),$$

where α_e and t_e are the experimental values and α=α_0 at t=t_0.

3. Results

3.1. Isothermal analysis

Figs. 1–3 illustrate the types of α against time plots obtained for the complexes with *nmf*, *aa* and *nma*, respectively, at different constant temperatures. The plots are initially approximately linear over an appreciable α range (e.g. $0.00 \leq \alpha \leq 0.35$), before becoming deceleratory. The kinetic models which gave acceptable descriptions of the isothermal results were established using several methods.

3.1.1. Rate (v=dα/dt) vs. time and rate vs. α plots

Plots of rate vs. time and rate vs. alpha (not illustrated) calculated from the data shown in Figs. 1–3

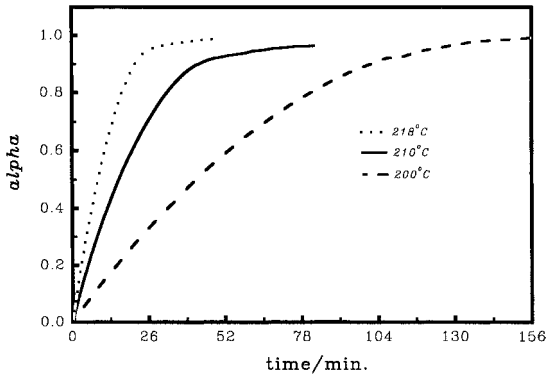

Fig. 1. Typical alpha vs. time plots for the decomposition of Ni(*nmf*)Cl_2 at different constant temperatures.

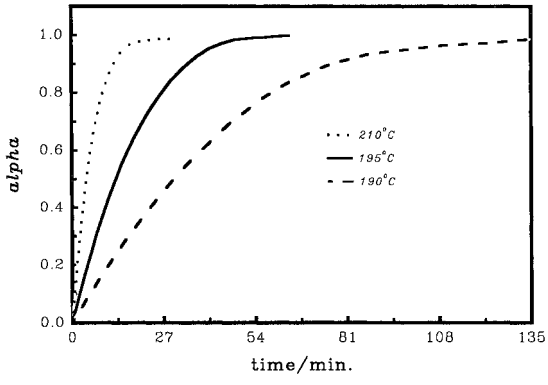

Fig. 2. Typical alpha vs. time plots for the decomposition of Ni(*aa*)Cl_2 at different constant temperatures.

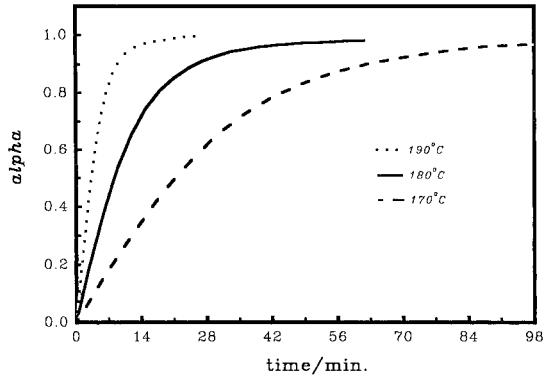

Fig. 3. Typical alpha vs. time plots for the decomposition of Ni(*nma*)Cl_2 at different constant temperatures.

Table 1
Arrhenius parameters for the isothermal decomposition of $NiLCl_2$ calculated using different methods of kinetic analysis

Models	α-range	E_a/kJ mol^{-1}	r	ln(A/s^{-1}) [a]
Zero-order				
Ni(*nmf*)Cl_2	0.00–0.30	137±9	0.9341	26.5±0.1
Ni(*aa*)Cl_2	0.00–0.30	148±11	0.9180	30.6±0.2
Ni(*nmf*)Cl_2	0.00–0.30	146±6	0.9741	13.8±0.1
Half-lives				
Ni(*nmf*)Cl_2	—	138±9	0.9364	(27.4±0.1)
Ni(*aa*)Cl_2	—	144±11	0.9172	(26.6±0.1)
Ni(*nma*)Cl_2	—	145±6	0.9750	(13.9±0.1)
R2 model				
Ni(*nmf*)Cl_2	0.00–0.95	142±8	0.9468	27.7±0.1
Ni(*aa*)Cl_2	0.00–0.95	138±10	0.9239	27.6±0.1
Ni(*nma*)Cl_2	0.00–0.85	145±9	0.9454	13.7±0.1
R3 model				
Ni(*nmf*)Cl_2	0.00–0.95	142±8	0.9456	27.0±0.1
Ni(*aa*)Cl_2	0.00–0.95	137±10	0.9232	30.0±0.1
Ni(*nma*)Cl_2	0.00–0.85	151±8	0.9536	14.1±0.1
v_{max} *based*				
Ni(*nmf*)Cl_2	—	124±5	0.9711	(23.3±0.1)
Ni(*aa*)Cl_2	—	123±10	0.9064	(21.5±0.1)
Ni(*nma*)Cl_2	—	144±5	0.9819	(13.7±0.1)
F1 eqn				
Ni(*nma*)Cl_2	0.00–0.95	150±9	0.9410	14.5±0.1
B2 eqn				
Ni(*nma*)Cl_2	0.05–0.85	147±7	0.9663	31.7±0.2

[a] The values in parentheses include ln{$g(\alpha)$}.

were examined and compared with plots expected for the main deceleratory models [3]. Estimated values of $t_{max/2}$, the time taken for the rate to drop to half its maximum value [3] at the different temperatures were plotted as ln{1/($t_{max/2}$)} against 1/T and the apparent activation energies calculated from the slope are presented in Table 1.

3.1.2. Zero-order approximation

If a rate equation of the simple reaction order type

$$d\alpha/dt = kf(\alpha) = k(1-\alpha)^n \quad (1)$$

applies, then when α is small, $(1-\alpha)\approx 1$ and $(1-\alpha)^n\approx 1$, so that

$$d\alpha/dt \approx k$$

Slopes of the initially linear portions of Figs. 1–3 were determined using a least-squares fit. Arrhenius plots were constructed using these approximately zero-order rate coefficients (k) calculated over the most extensive α range found to give acceptable straight lines. The calculated apparent activation energies are given in Table 1, for the complexes with *nmf*, *aa* and *nma*.

3.1.3. Plots of ln(rate) against ln(1−α)

Alternatively, if Eq. (1) applies, a plot of ln(rate) against ln(1−α) will be linear, with slope n (the apparent order of reaction), and intercept ln(k). Application of this test [4] to the *nmf*, *aa* and *nma* complexes gave n values from 0.510 to 0.731 (*nmf*, 200–245°C); from 0.533 to 0.959 (*aa*, 190–235°C); and from 0.590 to 0.960 (*nma*, 170–210°C). There was no distinguishable trend in the values of n with temperature and these values did not permit reliable discrimination between the R2 (n=0.50), R3 (n=0.67) or F1 (n=1.00) models.

3.1.4. Reduced-time plots

For an isokinetic process, if the times required to attain a set value of α (e.g., α=0.50) at several different (isothermal) temperatures are determined ($t_{0.50}$), then plots of α against reduced time (t_{red}= $t/t_{0.50}$) can be prepared [5] (see Figs. 4–6, for *nmf*, *aa* and *nma*, respectively). Comparison of the experimental reduced-time plots with theoretical curves for a selected number of kinetic expressions, did not provide an unambiguous choice of rate equation (e.g., R3, R2 or F1) for the experimental data. Values

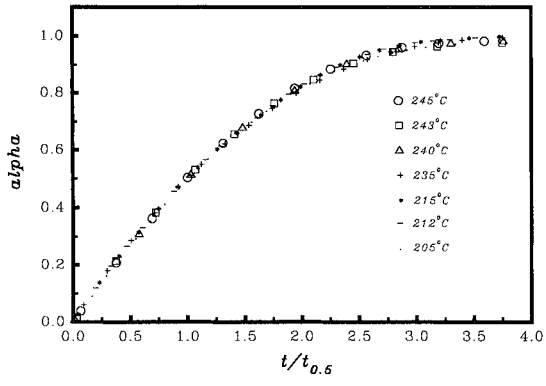

Fig. 4. Comparison of reduced-time plots for the decomposition of Ni(*nmf*)Cl_2 at different constant temperatures.

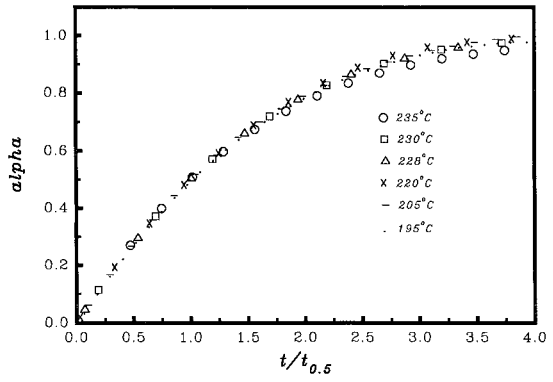

Fig. 5. Comparison of reduced-time plots for the decomposition of Ni(*aa*)Cl_2 at different constant temperatures.

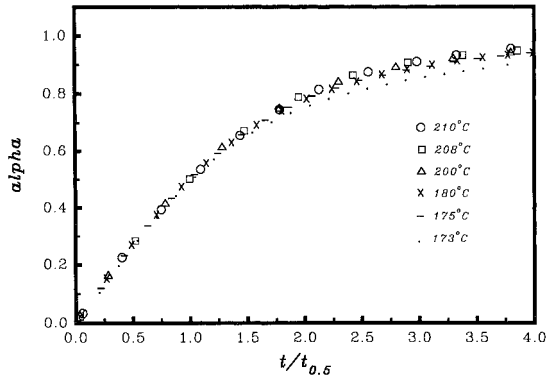

Fig. 6. Comparison of reduced-time plots for the decomposition of Ni(*nma*)Cl_2 at different constant temperatures.

of $t_{0.50}$ estimated at several different (isothermal) temperatures were used in Arrhenius-type plots, $\{\ln(1/t_{0.50})$ against $1/T\}$, to evaluate the apparent activation energies of the decompositions, without the necessity for identifying the kinetic model [3]. The apparent activation energies calculated from the slope are included in Table 1. The intercept includes $\ln\{g(\alpha)\}$ and does not directly yield the pre-exponential factor.

3.1.5. *Plots of the integrated rate functions, g(α), against time*

The linearity of plots of the integrated rate functions, $g(\alpha)$, against time (Figs. 7–9, for *nmf*, *aa* and *nma*, respectively) over the ranges $0.00 \leq \alpha \leq 0.85$ and $0.00 \leq \alpha \leq 0.95$ was assessed using the standard error of

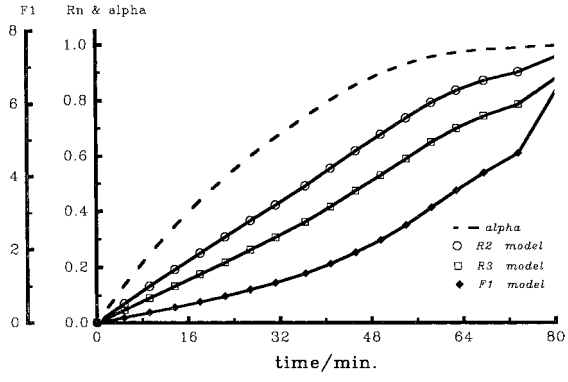

Fig. 7. Plots of $g(\alpha)$ vs. time for the isothermal decomposition of Ni(*nmf*)Cl_2 using the R3, R2 and F1 models.

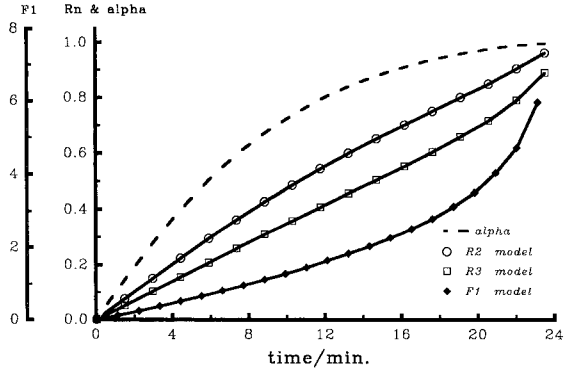

Fig. 8. Plots of $g(\alpha)$ vs. time for the isothermal decomposition of Ni(*aa*)Cl_2 using the R3, R2 and F1 models.

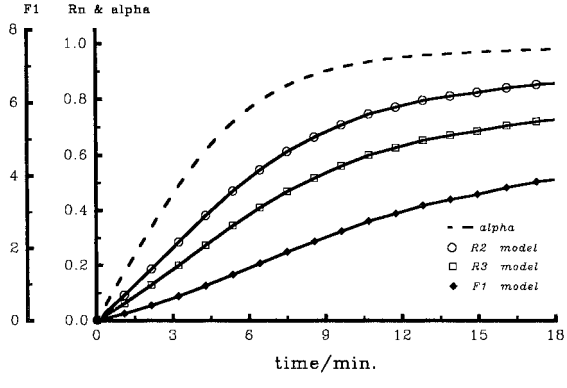

Fig. 9. Plots of $g(\alpha)$ vs. time for the isothermal decomposition of Ni(*nma*)Cl_2 using the R3, R2 and F1 models.

the slope (s_b) and the correlation coefficient (r) [6]. It was again difficult to distinguish between applicability of the R2 and R3 models. Arrhenius plots constructed using k values from the acceptable $g(\alpha)$ functions gave the apparent activation energies and the pre-exponential factors presented in Table 1.

3.1.6. Comparison of model with experiment

Values of k, determined using the R2, R3 or F1 models over the most extensive α range, were subsequently used in the appropriate integrated expressions [7] to calculate expected α_{calc} vs. time curves for comparison with experimental α_e vs. time curves. Typical results are shown in Figs. 10 and 12 for the *nmf*, *aa* and *nma* complexes, respectively. Comparison often permitted a distinction between applicability of the R2 and R3 models.

3.1.7. An empirical model

The experimental isothermal rate vs. alpha curves for the Ni(*nma*)Cl_2 complex (Fig. 13) have concave down curvature and rather abrupt completion, which is not provided for in the usual range of kinetic models [7]. An empirical rate equation which could give rise to this type of isothermal rate-time curve is

$$v = d\alpha/dt = v_{max}[1 - (kt)^b]$$

(which will be referred to as the B2 expression). Writing

$$v_r = v/v_{max} = 1 - (kt)^b$$

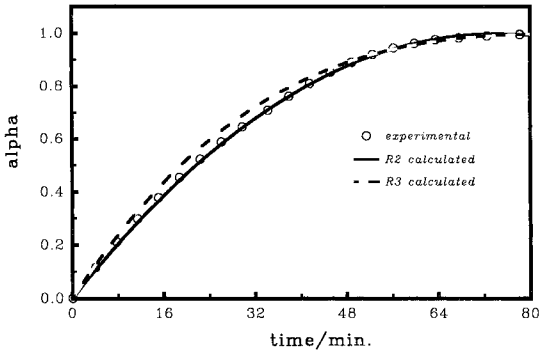

Fig. 10. Plots of α_{calc} vs. time using the R2 and R3 models, compared with α_e vs. time data for the isothermal decomposition of Ni(*nmf*)Cl_2.

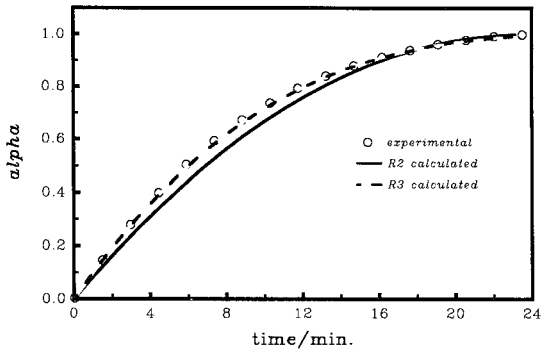

Fig. 11. Plots of α_{calc} vs. time using the R2 and R3 models, compared with α_e vs. time data for the isothermal decomposition of Ni(*aa*)Cl_2.

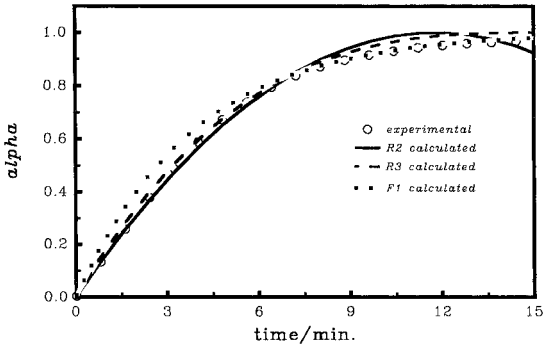

Fig. 12. Plots of α_{calc} vs. time using the R2, R3 and F1 models, compared with α_e vs. time data for the isothermal decomposition of Ni(*nma*)Cl_2.

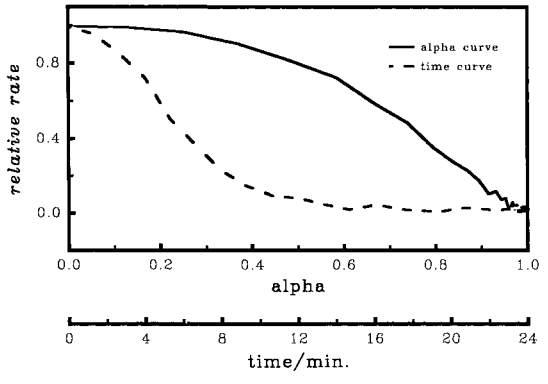

Fig. 13. Plots of rate vs. alpha and rate vs. time for the isothermal decomposition of Ni(*nma*)Cl_2 at 190°C.

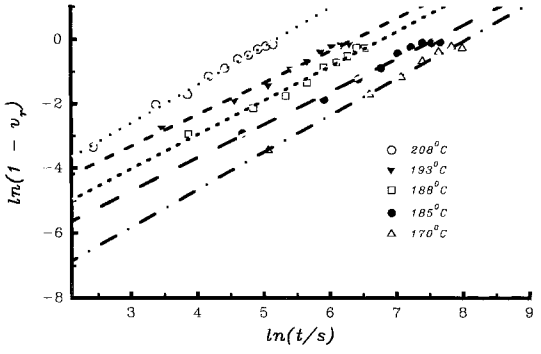

Fig. 14. Plots of $\ln(1-v_r)$ vs. $\ln(t)$ for the isothermal decomposition of Ni(*nma*)Cl_2 at different constant temperatures for the range $0.05<\alpha<0.85$.

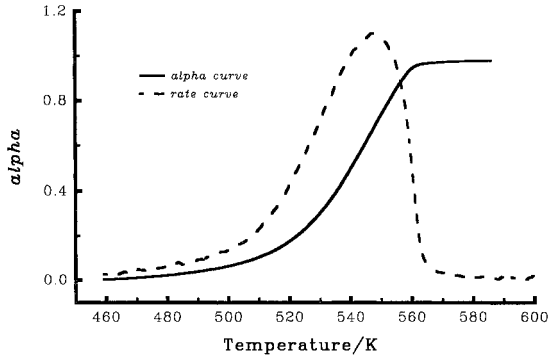

Fig. 15. Plots of α vs. T and rate vs. T for the non-isothermal decomposition of Ni(*nmf*)Cl_2 heated in nitrogen at 20°C min^{-1}.

and hence

$$\ln(1 - v_r) = b\ln(t) + b\ln(k)$$

A plot of $\ln(1-v_r)$ against $\ln(t)$ for Ni(*nma*)Cl_2, Fig. 14, indicated that the value of b is ≈ 2. Plots of $(1-v_r)^{1/b}$ against time, using $b=2$, yielded approximately straight lines. Arrhenius plots, using rate coefficients from the most extensive acceptable α range, gave the apparent activation energies and the pre-exponential factors included in Table 1.

3.2. Non-isothermal analysis

Three different methods of non-isothermal analysis were used: the Coats and Redfern [8], Borchardt and Daniels [9], and Kissinger [10] methods.

3.2.1. The Coats and Redfern method [8]

A plot of $\ln[g(\alpha)/T^2]$ against $1/T$ should give a straight line when the correct $g(\alpha)$ is chosen. $g(\alpha)$ functions corresponding to 'reaction orders' $n=0$, 0.33, 0.50, 0.67, 1.00 and 2.00 were tested. The programmed-temperature TG run for Ni(*nmf*)Cl_2 gave the α vs. temperature (T) and rate ($v=d\alpha/dt$) vs. T plots shown in Fig. 15. Fig. 16 shows the Coats–Redfern analysis based on the TG data of Fig. 15. The best straight lines are obtained over the 500–550 K interval, using the smaller values of n, i.e. 0, 0.33, 0.50 and 0.67. The calculated values of E_a are given in Table 2.

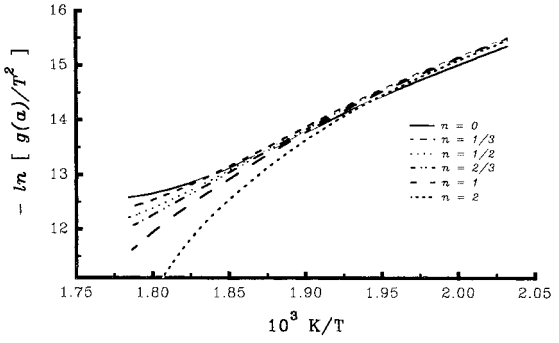

Fig. 16. Arrhenius-type plots for the non-isothermal decomposition of Ni(*nmf*)Cl_2 using the Coats and Redfern method. The temperature range used is 500–560 K.

3.2.2. The Borchardt and Daniels method [9]

This method is based on the calculation of rate constants as $k=[\beta(d\alpha/dT)/f(\alpha)]$. Choosing $f(\alpha)=(1-\alpha)^n$ leads to $k=[\beta(d\alpha/dT)/(1-\alpha)^n]$ and

$$\ln(k) = \ln[\beta(d\alpha/dT)/(1-\alpha)^n] = -E_a/RT + \ln(A)$$

where β is the (constant) heating rate. Plots of $\ln(k)$ vs. $1/T$ for different values of n=0, 0.33, 0.50, 0.67, 1.00 or 2.00 are shown in Fig. 17. The criterion of the best linearity indicated n=0.67 as the most probable order (Table 3).

3.2.3. The Kissinger method [10]

This method is based on the equation

$$\ln(\beta/T^2)_{max} = -E_a/RT_{max} + \ln(AR/E_a)$$

Table 2
Apparent activation energies calculated for the non-isothermal decomposition of Ni(*nmf*)Cl_2 using the Coats–Redfern method

Order n	E_a/kJ mol^{-1}	r	Constant, a [a]
(a) α-range: 0.06–0.80, i.e. 500–550 K			
0	104.7±0.3	0.9988	10.15±0.03
1/3	113.0±0.3	0.9987	11.98±0.03
1/2	116.7±0.4	0.9981	12.87±0.04
2/3	120.8±0.5	0.9971	13.83±0.05
1	129.2±0.8	0.9940	15.82±0.07
2	157.6±1.9	0.9769	22.55±0.17
(b) α-range: 0.06–0.90, i.e. 500–558 K			
0	102.6±0.4	0.9974	9.66±0.04
1/3	112.4±0.3	0.9988	11.83±0.03
1/2	116.9±0.3	0.9985	12.92±0.03
2/3	122.0±0.5	0.9974	14.11±0.05
1	132.7±0.8	0.9931	16.63±0.08
2	170.4±2.5	0.9644	25.54±0.24
(c) α-range: 0.06–0.95, i.e. 500–560 K			
0	100.7±0.5	0.9954	9.21±0.05
1/3	111.5±0.3	0.9986	11.62±0.03
1/2	116.8±0.3	0.9987	12.88±0.03
2/3	122.7±0.4	0.9976	14.26±0.05
1	135.3±0.9	0.9920	17.23±0.10
2	181.8±3.1	0.9502	28.20±0.33

[a] $a = -\ln[AR/\beta E_a)(1-2RT/E_a)]$.

Table 3
Apparent activation energies calculated for the non-isothermal decomposition of Ni(*nmf*)Cl_2 using the modified Borchardt–Daniels method

Order n	E_a/kJ mol^{-1}	r	ln(A)
(a) α-range: 0.06–0.80, i.e. 500–552 K			
0	96.4±0.7	0.9865	23.28±0.13
1/3	118.8±0.8	0.9920	28.56±0.07
1/2	127.7±0.5	0.9972	30.66±0.05
2/3	136.5±0.3	0.9993	32.76±0.03
1	154.2±0.6	0.9974	36.96±0.06
2	207.2±2.6	0.9749	49.55±0.23
(b) α-range: 0.06–0.90, i.e. 500–558 K			
0	90.36±2.0	0.9190	21.85±0.20
1/3	113.1±1.1	0.9839	27.24±0.11
1/2	124.6±0.6	0.9954	29.94±0.06
2/3	136.0±0.3	0.9994	32.64±0.03
1	158.8±0.9	0.9949	38.03±0.09
2	227.2±3.7	0.9563	54.21±0.36
(c) α-range: 0.06–0.95, i.e. 500–560 K			
0	78.8±2.8	0.8088	19.18±0.30
1/3	106.2±1.6	0.9576	25.63±0.18
1/2	119.9±1.1	0.9855	28.78±0.11
2/3	133.6±0.6	0.9967	32.10±0.06
1	161.1±0.9	0.9943	38.56±0.10
2	243.3±4.4	0.9426	57.93±0.47

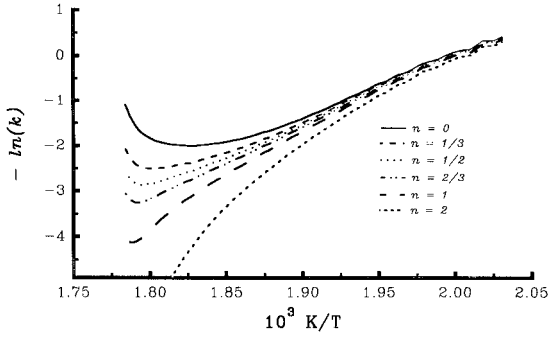

Fig. 17. Arrhenius plots for the non-isothermal decomposition of Ni(*nmf*)Cl_2 using rate coefficients from the modified Borchardt–Daniels method. The temperature range used is 500–560 K.

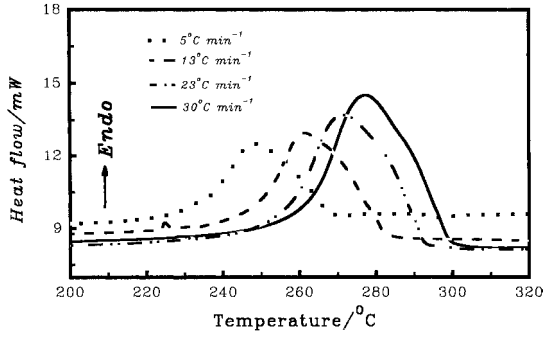

Fig. 18. DSC curves for the non-isothermal decomposition of Ni(*nmf*)Cl_2 heated at different constant heating rates.

in which the subscript max signifies 'peak' quantities. Therefore, a plot of $\ln(\beta/T^2)_{max}$ vs. $1/T_{max}$ for several dynamic curves obtained at different heating rates (β) should yield a straight line of slope $-E_a/R$.

Typical DSC curves obtained at different heating rates are shown in Fig. 18. Fig. 19 shows the plot of $\ln(\beta/T^2)_{max}$ vs. $1/T_{max}$. The calculated kinetic parameters are given in Table 4.

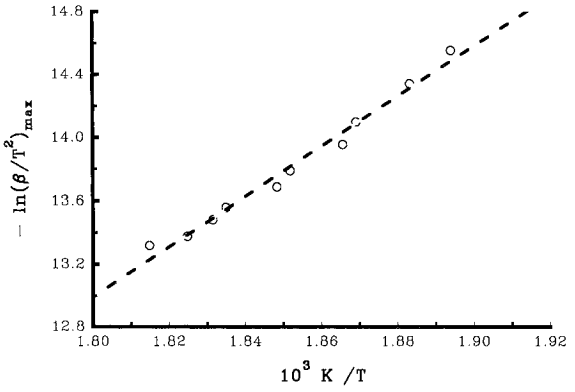

Fig. 19. Arrhenius-type plot for the non-isothermal decomposition of Ni(*nmf*)Cl_2 using the Kissinger method on the DSC data from Fig. 18.

Table 4
Non-isothermal DSC data for the decomposition of Ni(*nmf*)Cl_2: (β and T_{max}) and the apparent activation energy calculated using the Kissinger method

β/°C min^{-1}	T_{max}/K	$-\ln(\beta/T^2)_{max}$
5	522	15.00
8	528	14.55
10	531	14.34
13	535	14.10
15	536	13.96
18	540	13.79
20	541	13.69
23	545	13.56
25	546	13.48
28	548	13.38
30	551	13.32
E_a/kJ mol^{-1}=141±6	r=0.9848	ln(A)=27.2±0.7

4. Discussion

For the kinetic study, only those few complexes that decomposed in a single step without decomposition of the released ligand were chosen. These were the $NiLCl_2$ complexes, where L=*N*-methylformamide (*nmf*), acetamide (*aa*) or *N*-methylacetamide (*nma*).

4.1. $NiLCl_2$ isothermal kinetic results

Plots of α against time are deceleratory and are best described by either the R2, R3 or F1 expressions. The early portion of the rate against α curves is consistent with an approximately zero-order initial process. The plots of ln(rate) against ln(1−α) are approximately linear over the range of $0.03 \leq \alpha \leq 0.90$. The apparent orders derived lie in the region expected for the R2 (0.50), R3 (0.67) and F1 (1.00) models. Good agreement was obtained on plotting the experimental values of alpha (α_e) against reduced time ($t/t_{0.5}$), indicating that the reactions are isokinetic over the temperature ranges studied (see Figs. 4–6). Comparison of experimental data in the form of α against $t/t_{0.5}$, with similar curves calculated for various models indicated better coincidence ($0.00 \leq \alpha \leq 0.95$) with the contracting geometry rate expressions than with the first-order rate equation. The R3 and R2 models were difficult to distinguish between, particularly for the decomposition of the Ni(*nmf*)Cl_2 complex.

For the Ni(*aa*)Cl_2 and Ni(*nma*)Cl_2 complexes, highest correlation coefficients and smallest standard errors of slope were obtained when using the contracting-volume (R3) equation. Obedience to the F1 equation improved notably, for all the complexes, on going to higher α values (>0.95). Plots of α_{calc} (for n=1.00, 0.50 and 0.67) and α_e against time indicated best fit for n=0.67 in the most extensive α range in all the complexes (see Figs. 10–12). The fit of the kinetic data to deceleratory-yield–time curves suggests that, at constant temperature, progress of the reactions is controlled by inward motion of the reactant–product interface.

The Arrhenius parameters, as obtained by the different methods of isothermal analysis, were estimated and compared for the reactions. The mean E_a values obtained are shown in Table 5.

Some trends which emerged from inspection of the E_a values include:

- Magnitudes of the apparent activation energies for a particular reaction are not very sensitive to the kinetic model used to calculate the rate coefficients.
- E_a values obtained for Ni(*nmf*)Cl_2 are similar to those of Ni(*aa*)Cl_2.

Largest values are obtained for Ni(*nma*)Cl_2 using either of the models.

- Non-mechanistic approaches based on estimated values of $t_{0.5}$ or $t_{max/2}$ give rise to E_a values that are in good agreement with values calculated using mechanistic approaches. The apparent activation energies derived on the basis of the $t_{max/2}$ data are,

Table 5
Comparison of the mean E_a values calculated for the isothermal decompositions of the $NiLCl_2$ complexes using different methods of analysis

Parameters	Ni(*aa*)Cl_2	Ni(*nma*)Cl_2	Ni(*nmf*)Cl_2
Model R3			
E_a/kJ mol^{-1}	141	149	141
r	0.927	0.959	0.942
Model R2			
E_a/kJ mol^{-1}	142	146	141
r	0.927	0.954	0.942
Zero-order			
E_a/kJ mol^{-1}	148	146	137
r	0.918	0.974	0.934
Model F1			
E_a/kJ mol^{-1}	—	149	—
r		0.954	
Half-life			
E_a/kJ mol^{-1}	144	145	138
r	0.917	0.975	0.936
$t_{max/2}$			
E_a/kJ mol^{-1}	123	144	124
r	0.906	0.982	0.971
B2 equation			
E_a/kJ mol^{-1}	—	144	—
r		0.969	

however, slightly and consistently lower than those from the other methods of analysis.

The fact that several different determinations of E_a from isothermal experiments lead to comparable values adds confidence to the methods employed.

Apparent activation energies for the decomposition of other amide complexes have been reported [11,12]. Making allowances for the different experimental conditions, there are noteworthy similarities between values of E_a calculated in the present study (Table 5) and values reported by other workers. For example, Carstens et al. [11] fitted isothermal decomposition data for UO_2(*aa*)F_2 and UO_2(*nma*)F_2 to the contracting-area (R2) equation, and reported E_a values of 125 and 150 kJ mol^{-1}. In a related study, Siracusa et al. [12] found an E_a value of 123 kJ mol^{-1} for the decomposition of UO_2(*aa*)F_2.

4.2. *Ni(nmf)Cl_2 non-isothermal kinetic results*

The linearities of Coats–Redfern plots with n=0.33, 0.50 or 0.67 are similar (Table 3). It was therefore not possible to deduce, unambiguously, the proper form of $g(\alpha)$. Other authors [13,14] have shown that the linearity is a necessary, but insufficient, criterion to assign the correct form of $g(\alpha)$. The Borchardt–Daniels plots corresponding to n=0.67 gave the best straight lines (Fig. 17). This is in agreement with the choice of the R3 equation based on results of the isothermal experiments.

An apparent activation energy of 141±6 kJ mol^{-1} was obtained using the Kissinger method. The E_a value is similar to that derived from the isothermal analysis using the R3 or R2 model. Agreement between E_a values calculated using the Kissinger method and isothermal values has been reported in Refs. [15,16].

4.3. *Comparison between E_a and ΔH_L values for the decompositions of the $NiLCl_2$ complexes*

The dependence of E_a values on the nature of the amide ligands was examined using the mean values obtained from the R3 and R2 models. Results indicate the order:

$$N\text{-methylformamide} \sim \text{acetamide} < N\text{-methylacetamide}$$

This sequence suggests an increase in E_a with increase in basicity of the amide ligand.

ΔH values may contain contributions from several distinct chemical processes such as bond rupture, crystallization of the solid products and desorption of the gaseous products. E_a is expected to incorporate the maximum energy required for bond cleavage. The calculated E_a values are lower than the corresponding ΔH_L values, suggesting that the rate-controlling event is the nickel–amide bond cleavage [17–19]. It has been suggested [18,20–25] that E_a provides an assessment of the strength of metal–volatile ligand bond for decompositions that are chemically controlled. Farran et al. [22] reported an increase in E_a values with increase in basicity of the alkyl-substituted pyridine from decomposition studies of the PdL_2Cl_2 complexes. Akhavein et al. [23] reported a similar trend from thermal decomposition studies of $AgL_2(NO_3)$

complexes with several alkyl-substituted pyridines. The E_a trend found in the present study is consistent with the above findings. In contrast, ΔH_L, T_e and T_{max} (where T_e is the extrapolated onset temperature and T_{max} the temperature at maximum decomposition rate) give an assessment of the steric factors. No simple correlation was found between E_a and the physical parameters investigated [1].

References

[1] A.N. Nelwamondo, D.J. Eve, M.E. Brown, Thermochim. Acta, pp 165 (this issue).
[2] A. Savitsky, M.J.E. Golay, Anal. Chem. 36 (1964) 1627.
[3] M.E. Brown, A.K. Galwey, Anal. Chem. 61 (1989) 1136.
[4] J.H. Flynn, J. Thermal Anal. 34 (1988) 367.
[5] J.H. Sharp, G.W. Brindley, B.N.N. Achar, J. Amer. Ceram. Soc. 49 (1966) 379.
[6] M.E. Brown, A.K. Galwey, Thermochim. Acta 29 (1979) 129.
[7] M.E. Brown, D. Dollimore, A.K. Galwey, in: C.H. Bamford, C.J. Tipper (Eds.), Reactions in the Solid State, Comprehensive Chemical Kinetics, vol. 22, Elsevier, Amsterdam, 1980.
[8] A.W. Coats, J.P. Redfern, Nature (London) 201 (1964) 68; Polym. Lett. 3 (1965) 917.
[9] H.J. Borchardt, F.J. Daniels, J. Am. Chem. Soc. 79 (1957) 41.
[10] H.E. Kissinger, J. Res. Nat. Bur. Stand. 57 (1956) 217; Anal. Chem. 29 (1957) 1702.
[11] P.A.B. Carstens, T.P. Knoetze, C.P.J. van Vuuren, Thermochim. Acta 128 (1988) 237.
[12] G. Siracusa, L. Abate, R. Maggiore, Thermochim. Acta 56 (1982) 333.
[13] J.M. Criado, J. Morales, Thermochim. Acta 16 (1976) 382; 19 (1977) 305.
[14] A.J. Kassman, Thermochim. Acta 84 (1985) 89.
[15] L.R. Ocone, J.R. Soulen, B.P. Block, J. Inorg. Nucl. Chem. 15 (1960) 79.
[16] Y.P. Khanna, E.M. Pearce, J. Thermal Anal. 26 (1983) 107.
[17] E. Jona, T. Sramko, P. Ambrovic, J. Gazo, J. Thermal Anal. 4 (1972) 153.
[18] E. Jona, V. Jesenak, T. Sramko, J. Gazo, J. Thermal Anal. 5 (1973) 57.
[19] E. Jona, V. Jesenak, T. Sramko, J. Gazo, J. Thermal Anal. 5 (1973) 389.
[20] G. Beech, J. Chem. Soc. (A) (1969) 1903.
[21] R.P. Bonomo, S. Gurrieri, S. Musumeci, E. Rizzarelli, G. Siracusa, Thermochim. Acta 9 (1974) 373.
[22] R. Farran, J.E. House, J. Inorg. Nucl. Chem. 34 (1972) 2219.
[23] A. Akhavein, J.E. House, J. Inorg. Nucl. Chem. 32 (1970) 1479.
[24] S. Gurrieri, R. Maggiore, S. Musumeci, G. Siracusa, Thermochim. Acta 11 (1975) 73.
[25] R.P. Bonomo, S. Gurrieri, S. Musumeci, E. Rizzarelli, G. Siracusa, Thermochim. Acta 10 (1974) 119.